INVESTIGATION OF FAILURE BEHAVIOR IN HONEYCOMB SANDWICH PANEL CONTAINING INTERFACIAL DEBONDING

Shi-dong Pan, Lin-Zhi Wu, Shan-Yi Du
Center for Composite Materials, Harbin Institute of Technology

Keywords: *interfacial debonding; interlaminar delamination; kinking; Tsai-Hill failure criterion; cohesive zone model*

Abstract

A series of experiments are designed and performed to investigate the failure modes of honeycomb sandwich containing facesheet/core interfacial debonding. In terms of double cantilever beam (DCB) and single leg bending (SLB) experiments, new fracture modes, namely IKPs (initiation of interlaminar delamination, kinking into facesheet and propagation of interlaminar delamination), are found. One new computational model based on the Tsai-Hill failure criterion and cohesive zone model is proposed to simulate the failure process of DCB and SLB tests of honeycomb sandwich specimens. The computational model is also used to predict the failure modes of honeycomb sandwich panels containing interfacial debonding under edgewise compressive (EC) loading. In our EC simulation, observation of the compression response has shown that the failure occurred by local buckling of the facesheet within the interfacial debonding region, followed by the initiation of interlaminar delamination between 45-degree ply and 0-degree ply, the fracture of 45-degree ply and the rapid propagation of interlaminar delamination between 45-degree ply and 0-degree ply, finished by the symmetrical global buckling of facesheets. Comparison with results of the EC test, it is clear that the new failure modes predicted in the simulation are also found in the EC test.

1 Introduction

Sandwich composite structures with stiff composite facesheets bonded to the low-density core material are widely used in man-made satellite, rocket, missile, automotive and aerospace. The main role of facesheets is to carry in-plane and bending loads. The core acts to separate the facesheets, increase the moment of inertia of the panel with little increasing in weight, and produce an efficient structure for resisting bending and buckling loads. Usually, the facesheets are made of carbon fibre reinforced laminate, and the core is made of lightweight cellular material including honeycomb core and foam core. In comparison with traditional stiffened panels, on one hand, sandwich structures have many advantages including high flexural rigidity and strength, ease of manufacture, improved stability and ease of repair; on the other hand, the ultimate carrying load capacity of honeycomb sandwich composites may be affected by the presence of flaws or defects that often occur during the process of manufacture, transportation and service[1]. The most common and dangerous defect is the facesheet/core interfacial debonding. In general, this kind of defects may lead to the significant strength reduction under compressive loading. With the increasing of loading, defects may propagate and ultimately precipitate the catastrophic failure of the entire sandwich structure.

Many researchers have investigated the facesheet/core interfacial debonding of sandwich composite structures by theoretical analysis and experiment. Prasad and Carlsson[2,3] have employed one modified DCB geometry and one sandwich shear fracture specimen to investigate the interfacial fracture toughness of aluminum facesheet and polymer foam sandwich structures. They investigated the influence of changes in core thickness, core materials and crack length on the total strain energy release rate, and found that the Mode I strain energy release rate dominates the fracture behavior. The tiled sandwich debond (TSD) has been proposed to study the mixed-mode fracture in sandwich beams[4]. Cantwell and Davies[5,6] have introduced the single cantilever beam (SCB) to investigate the facesheet/core debonding in balsa-

based and foam-based sandwich structures. Tests have showed that the crack propagation in sandwich materials occurs between the facesheet and core materials in one stable manner. Cantwell *et al.*[7] have developed a test geometry named as three-point-bending sandwich (TPBS) for characterizing debonding between the glass-polyester facesheet and the foam core in sandwich composite structures. Tests have shown that Mode I energy release rate dominated the failure of sandwich structures. Up to now, only few research works on the fracture test of honeycomb sandwich structures are involved. Ural *et al.*[8] have finished the flatwise tension test and the DCB test of honeycomb sandwich composites and found that the fracture toughness varies with the facesheet thickness and core materials and is also different for the bag and tool sides of panels for all types of specimens. In the literatures mentioned above, several kinds of typical fracture modes have been shown. For most of sandwich structures, the propagation of the interfacial debonding stays on the facesheet/core interface from the beginning to the end. But for some foamed sandwich structures, the crack diverges from the facesheet/core interface and kinks into the foam core after the considerable interfacial propagation. For some honeycomb sandwich structures, the crack also diverges from the facesheet/core interface and kinks into the interlaminar path between the composite plies of the facesheet after the considerable interfacial propagation. Park *et al.*[9] have studied the buckling and ultimate strengths of honeycomb sandwich plates and found that the facesheet is deformed symmetrically with respect to the centre line of the higher core. Gdoutos *et al.* [10] have investigated the facesheet wrinkling failures of sandwich columns under compression and found the facesheet wrinkling failures of foam core sandwich columns. Kwon *et al.* [11] have also investigated the compression failure of sandwich composites made of fibrous carbon-epoxy facesheet and foam core. Tests showed that overall buckling was the initial failure and core shearing occurred post-failure. Vadakke and Carlsson [12] have studied the in-plane compressive failure mechanism of foam cored sandwich specimens with an implanted through-width face/core debond and found that the specimens failed due to buckling of the debonded facesheet followed by rapid propagation of the debond.

Some researchers have also investigated the facesheet/core interfacial debonding in sandwich composite structures by cohesive crack models. The cohesive zone model was proposed by Dugdale[13] and Barenblatt[14] to investigate the nonlinear fracture process. Sayed *et al.*[15] have proposed computational models based on the cohesive layer concept to simulate the delamination growth on the facesheet/core interface and crack kinking into the sandwich core, respectively. Recently, the cohesive element approach has been proposed as a tool for simulating delamination propagation between the facesheet and the core with reasonable accuracy [16]. In comparison with experimental results, the cohesive layer models are able to capture the initiation and track the growth of the interfacial delamination.

In this paper, the failure modes of carbon fiber reinforced facesheet and aluminum alloy honeycomb core sandwich structures are investigated experimentally and numerically. The interlaminar peel strength of honeycomb sandwich specimens and the interlaminar shear strength of facesheet specimens are tested. The new fracture modes, namely *IKPs*, are observed in terms of the DCB and SLB experiments. The finite element method based on virtual crack closure technique is used to separate the reasonable value of Mode I and Mode II components of strain energy release rate measured in the SLB experiment. A computational model based on the Tsai-Hill failure criterion and cohesive zone model is proposed to simulate the fracture behavior of the DCB and SLB experiments, and results are compared with experiment. Then the computational model is also used to predict the failure modes of honeycomb sandwich panels containing interfacial debonding under EC loading. The predicted typical failure modes have been successfully observed in our EC test of honeycomb sandwich panels containing through-width interfacial debonding.

2 Experiment Investigations

2.1 Material Properties

The macroscopic mechanical properties of a honeycomb sandwich panel depond on cell size, cell wall thickness, facesheet material and facesheet thickness. In this work, the brand of the aluminum alloy honeycomb core is 3/16-5056P-0.0007, and the facesheets are made of carbon firber/epoxy resin laminates.

For the hexagonal aluminum alloy 5056 honeycomb core, the height of honeycomb core is 10mm, and the length of cell wall is 3mm. Owing to the requirements of manufacture, the honeycomb core consists of continuously corrugated ribbons of

thin foil in the x-direction. The foil ribbons are bonded together to form the honeycomb with a metal-to-metal adhesive over all longitudinal walls, so that these walls have the double thickness as compared with the inclined walls of honeycomb cells. Therefore, the structure properties of honeycomb core show directional characteristics. It is usual to refer to the x-direction and y-direction as the L direction and W direction, respectively. The elastic properties of the core material are known. However, the honeycomb cores have very different properties from the monolithic properties of the material from which they are made. One method of computing the effective modulus of the core is homogenization of the core. Homogenized properties of the core are given in Table 1.

Table 1. Material properties of core (MPa)

E_1=E_2	E_3	G_{12}	G_{13}	G_{23}
0.6	316	0.15	189	90

The facesheets are made of transversely isotropic stacking of 26-plies. The thickness of the single ply is 0.1mm.The stacking sequence of bag side and tool side of sandwich is [45/03/-45/03/-45/03/45]. The material properties of a single ply are tested and listed in Table 2.

Table 2. Material properties of ply (GPa)

E_1	E_2 =E_3	G_{12}	G_{13}	G_{23}
300	5.7	3.8	3.8	2.2

2.2 Flatwise tension test of honeycomb sandwich specimens

The flatwise tension test (FWT), as specified in ASTM Standard C 297-94[17], may be used to determine the peel strength of honeycomb sandwich specimens. Transmission of the loads to the honeycomb sandwich coupon is achieved by thick loading steel blocks bonded to the facesheets with the Brand J-39 adhesive. The specimen is dried at room temperature for more than 24 hours before testing. The FWT is performed on 26-ply, 80 x 80 mm honeycomb sandwich panel specimens using the Zwick testing machine (ZWICK100). The test is performed in displacement control with a rate of 0.50 mm/min at room temperature. Five specimens are tested at the present analysis.

In the present FWT experiment, not the interfacial debonding between facesheet and honeycomb core, but the interlaminar delamination between plies of facesheet is found. Therefore, it is shown that the peel strength of interfacial bonding between facesheet and honeycomb core is higher than the peel strength of interlaminar delamination between plies of facesheet. The interlaminar peel strength is 2.64MPa.

2.3 Shear Test of Facesheet Specimens

In order to determine the shear strength of interlaminar delamination of facesheet, the shear test may be used. Transmission of the loads to the facesheet coupon is achieved by thick shear loading steel blocks bonded to the facesheet with the Brand J-39 adhesive. The specimen is dried at room temperature for more than 24 hours before testing. The shear experiment is performed on 13-ply, 20 x 8 mm facesheet specimens using the Instron 5569 universal testing machine. The stacking sequence of facesheet is [45/0_3/-45/0_3/-45/0_3/45]. The test is performed in displacement control with a rate of 0.50 mm/min at room temperature. Five specimens are tested using this procedure. The interlaminar shear fracture behavior occurs between 45-degree ply and 0-degree ply. The interlaminar shear strength is 52.8MPa.

2.4 Double Cantilever Beam Test of Honeycomb Sandwich Specimens

The DCB test is one kind of valuable approach for determining fracture toughness. The DCB specimen consists of two rectangular legs with a pre-crack of known size embedded between facesheet referred to as the tool side and honeycomb core. The dimension of the honeycomb sandwich specimen is 200 x 30 x 12.6 mm, and the dimension of the pre-crack is 50 x 30 mm. In order to introduce a pre-crack, the Teflon insert with the thickness of 0.02 mm is embedded at the facesheet and the core before the process of cure. Steel end blocks with the dimension of 16 x 30 x 16 mm used as load transferring agents between the grip and the specimen are bonded to both top and bottom facesheets using Brand J-39 adhesive. The tool side of specimen is coated with typewriter correction fluid. The specimen is also dried at room temperature for more than 24 hours before testing. The test is performed in displacement control with a rate of 1.3mm/sec at room temperature. The brand of testing machine is Instron 5569 universal testing machine.

2.5 Single Leg Bending Test of Honeycomb Sandwich Specimens

The SLB test is one kind of valuable approach for determining interfacial or interlaminar fracture toughness. The specimen of SLB consists of two rectangular legs with a pre-crack of known size. In this work, the dimension of the tool side of the

honeycomb sandwich specimen is 180x25x1.3 mm, and the dimension of the bag side is 150x25x1.3 mm. In order to introduce a pre-crack with dimension 20 x 25mm, the Teflon insert with the thickness of 0.02 mm is embedded between the facesheet and the core before the process of cure. The specimen is dried at room temperature for more than 24 hours before testing. The tool side of specimen is coated with typewriter correction fluid. In the actual test, the effective span of honeycomb sandwich beam specimens is 140 mm, and the dimension of the pre-crack is 30x25 mm^2. The test is also performed in displacement control with a rate of 0.5mm/min at room temperature. The brand of testing machine is also Instron 5569 universal testing machine.

2.6 Calculation and Separation of Strain Energy Release Rate

The critical strain energy release rate during the crack propagation may be expressed as

$$G_c = \frac{\int_0^{\delta} p d\delta}{B\Delta a} \qquad (1)$$

Here G_c is the critical strain energy release rate, p is the external load(for the loading path, it is positive; for the unloading path, it is negative), δ is the displacement, B is the width of specimen and Δa is the incremental crack length during the process of test. For the SLB fracture test, the energy required for crack growth, $\int_0^{\delta} p d\delta$, may be calculated according to the area enclosed by the loading-unloading path. The incremental crack length of specimen, Δa , may be measured by the microscopic Olympus SZX12. The interlaminar delamiantion energy release rates of DCB and SLB tests are 458N/m and 512N/m, respectively.

The energy release rate measured by the SLB test consists of two parts G_I and G_{II} (i.e. the opening Mode I and the shearing Mode II). The virtual crack closure technique is an approximate method to separate the values of Mode I and Mode II components of the strain energy release rate. Two steps are needed to obtain the components of strain energy release rate in the numerical simulation. The nodal forces at the crack tip just prior to crack growth are determined in the first step. In the second step, the relevant crack tip nodes are released to come into being the required corresponding nodal displacements. The nodal forces obtained in the first step are the forces required to close the crack. The work done during this process can then be obtained by multiplying one-half of the nodal forces with the corresponding displacements. Thus, the energy release rate may be expressed as

$$G = \frac{1}{2B\Delta a}\left[F_z^c\left(u_z^e - u_z^f\right) + F_{zx}^c\left(u_x^e - u_x^f\right)\right] \qquad (2)$$

Here F_z^c and F_{zx}^c are the nodal forces of node c in Fig. 1 (a), $u_z^e - u_z^f$ and $u_x^e - u_x^f$ are the relative nodal displacements of nodes e and f in Fig. 1 (b).

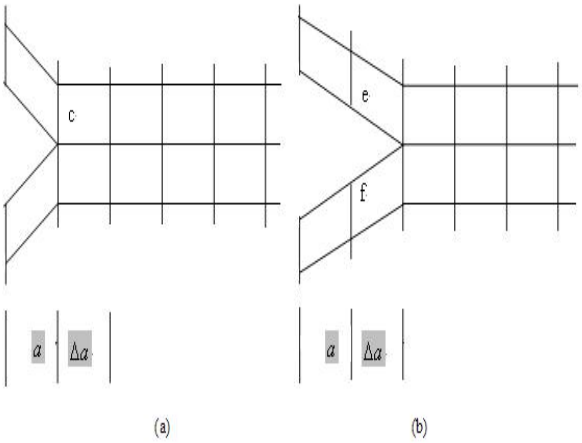

Fig. 1 Finite element mesh: (a) Before crack opening and (b) After crack opening

The components of strain energy release rate can be obtained by separating the nodal work into its corresponding components.

$$G_I = \frac{1}{2B\Delta a}F_z^c\left(u_z^e - u_z^f\right) \qquad (3)$$

and

$$G_{II} = \frac{1}{2B\Delta a}F_{zx}^c\left(u_x^e - u_x^f\right) \qquad (4)$$

Thus, the ratio of the Mode II strain energy release rate to the Mode I strain energy release rate may be written as

$$\frac{G_{II}}{G_I} = \frac{F_{zx}^c\left(u_x^e - u_x^f\right)}{F_z^c\left(u_z^e - u_z^f\right)} \qquad (5)$$

For the DCB test, the Mode II strain energy release rate is only about 5 percent of the Mode I strain energy release rate. And for the SLB test, he

Mode II strain energy release rate is about 25 percent of the Mode I strain energy release rate.

The crack of the SLB test may be considered as mix-mode. The dependence of the fracture energy release rate on the mix-mode crack can be defined based on a power law fracture criterion. The power law criterion means that the failure under mixed-mode conditions is governed by a power law interaction of the energy release rate required to cause the failure in the individual (normal and shear) modes. It is given by

$$\frac{G_I}{G_I^C}+\frac{G_{II}}{G_{II}^C}=1 \tag{6}$$

In the above expression, the quantities G_I and G_{II} refer to the components of strain energy release rate in the normal and shear directions, respectively. The quantities G_I^C and G_{II}^C refer to the critical strain energy release rates which cause the failure of the Mode I and Mode II, respectively.

As for the DCB experiment, the power law fracture criterion may be further expressed as

$$\frac{G_I^{DCB}}{G_I^C}+\frac{G_{II}^{DCB}}{G_{II}^C}=1 \tag{7}$$

Here the quantities G_I^{DCB} and G_{II}^{DCB} refer to the corresponding components of strain energy release rate during the process of the DCB test.

Similarly, for the SLB experiment, the power law fracture criterion may be expressed as

$$\frac{G_I^{SLB}}{G_I^C}+\frac{G_{II}^{SLB}}{G_{II}^C}=1 \tag{8}$$

Here the quantities G_I^{SLB} and G_{II}^{SLB} refer to the components of strain energy release rate during the process of the SLB test.

The quantities G_I^C and G_{II}^C may be expressed in terms of the equations (7) and (8) as

$$\begin{aligned} G_I^C &= 443N/m \\ G_{II}^C &= 1364N/m \end{aligned} \tag{9}$$

3 Computational methods

In the present experiment, the fracture of single ply and the initiation and propagation of interlaminar delamination are observed. The thickness of single ply is very thin, so its fracture behavior may be analyzed according to the Tsai-Hill failure criterion. For interlamianr delamination, the cohesive zone model is valid. Therefore, the computational model adopted in this paper is based on the Tsai-Hill failure criterion and the cohesive zone model.

3.1 Tsai-Hill failure criterion

Tsai-Hill failure criterion which is used to analyze the fracture behavior of single ply is expressed as

$$\frac{\sigma_1^2}{X^2}-\frac{\sigma_1\sigma_2}{X^2}+\frac{\sigma_2^2}{Y^2}+\frac{\tau_{12}^2}{S^2}=1 \tag{10}$$

Here X , Y and S are the ultimate strengths of single ply in the longitudinal, transverse, and shear directions, respectively, and σ_1, σ_2 and τ_{12} are the stress components in the longitudinal, transverse, and in-plane shear directions.

For the off-axis loading, the stress components may be written as

$$\begin{aligned} \sigma_1 &= \sigma_x \cos^2\theta \\ \sigma_2 &= \sigma_x \sin^2\theta \\ \tau_{12} &= -\sigma_x \sin\theta\cos\theta \end{aligned} \tag{11}$$

Here, θ is the angel between the material direction and the loading direction. Substituting Eq. (11) into Eq. (10), Tsai-Hill criterion can be further written as

$$\frac{\cos^4\theta}{X^2}+\left(\frac{1}{S^2}-\frac{1}{X^2}\right)\cos^2\theta\sin^2\theta+\frac{\sin^4\theta}{Y^2}=\frac{1}{\sigma_x^2} \tag{12}$$

3.2 Cohesive zone model

The cohesive zone model is characterized by a traction-separation law, which is a function of the fracture energy and strength. According to Griffith's theory, singular stresses are predicted at a crack tip. However, the cohesive model results in a non-singular stress at a crack tip. Here, considering the material properties of facesheet and computational efficiency of cohesive element, the relation between the effective stress and the effective strain within the cohesive element along the interlaminar delamination is assumed to be linear before the initiation of damage and nonlinear after the initiation of damage. As shown in Fig.2, the nominal stress-strain relation is expressed as the following relation

$$\sigma_i = E_i \varepsilon_i \quad \text{(Before damage initiation)} \qquad (13\text{-a})$$

$$\sigma_i = E_i \frac{\varepsilon_i^f / \varepsilon_i^{\max} - 1}{\varepsilon_i^f / \varepsilon_i^0 - 1} \varepsilon_i \quad \text{(After damage initiation, and } \varepsilon_i \le \varepsilon_i^f \text{)} \qquad (13\text{-b})$$

$$\sigma_i = 0 \qquad (\varepsilon_i \ge \varepsilon_i^f) \qquad (13\text{-c})$$

Here $i = I$ is the tension behavior of the traction-displacement relation, and $i = II$ is the shear behavior of the traction-displacement relation. Here, it is assumed that the tension behavior of Mode I and the shear behavior of Mode II are independent each other.

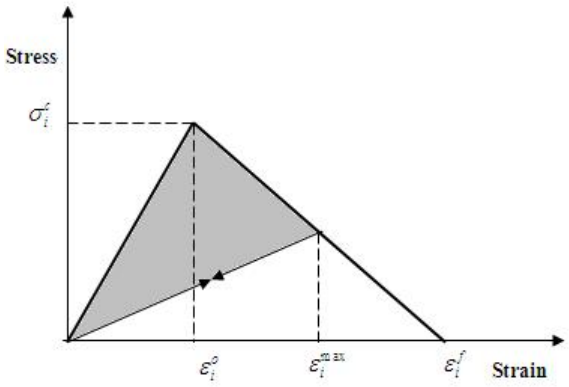

Fig. 2 Stress-strain relationship in the cohesive element

In the above expression, σ_i, ε_i and E_i are the nominal stress, strain and young's modulus of the cohesive elements, respectively, ε_i^f refers to the effective strain at complete failure, ε_i^0 refers to the effective strain at damage initiation, and $\varepsilon_i^{\max}$ refers to the maximum value of the effective strain determined by the loading history.

The magnitude of the separation energy stored in the cohesive elements per unit area is given by the area included by the stress-strain characteristic in the range $0 \le \varepsilon_i \le \varepsilon_i^{\max}$ at any instant. The strain energy release rate may be expressed as:

$$G_i = \int_0^{\varepsilon_i^{\max}} \sigma_i d\varepsilon_i \qquad (i = I, II) \qquad (14)$$

Here, the maximum value of G_i should be equal to the critical energy release rates based on the SLB experiment and the DCB experiment, so the critical energy release rates may be expressed as

$$G_i^C = \int_0^{\varepsilon_i^f} \sigma_i d\varepsilon_i = \frac{1}{2} \sigma_i^C * \varepsilon_i^f \qquad (i = I, II) \qquad (15)$$

Here σ_i^C is the interlaminar strength obtained from the flatwise tension tests and the shear tests, respectively, and may be given by:

$$\sigma_i^C = E_i * \varepsilon_i^0 \qquad (i = I, II) \qquad (16)$$

4 Modeling and Simulation

The facesheet named as the bag side is modelled with eight-node solid elements including 13 plies. The facesheet named as the tool side is also modelled with eight-node solid elements including 12 plies except 45-degree ply adjacent to honeycomb core. The 45-degree ply adjacent to honeycomb core is also modeled with eight-node solid elements, but those eight-node solid elements along the front of pre-crack are replaced with four-node shell elements which are used to calculate the fracture stress along the front of pre-crack. The equivalent elastic modulus and strength of single ply are recorded in Table 2.

For computational efficiency, eight-node solid elements are used to model the honeycomb core. The honeycomb core has strongly orthotropic properties and its in-plane elastic modulus are much lower than the put-of-plane ones (Table 1). Compared with the out-of-plane properties of honeycomb core, its in-plane properties have little effect on the behavior of the honeycomb panel. However, it should be noted that in-plane properties must be selected to avoid the negative definiteness of the constitutive model of the homogenized core.

The interlaminar delamiantion behavior is modelled by using eight-node cohesive elements based on the cohesive zone model. The cohesive element may be characterized with two parameters determined by tests, the interlaminar strength (σ_i^C) and the critical energy release rate (G_i^C). The effective strain at complete failure (ε_i^f) can be determined from these two parameters (G_i^C, σ_i^C) and Eq. (15). As mentioned earlier, the Young's modulus of the cohesive model may be determined according to the Young's modulus of facesheet. Once the Young's modulus of the cohesive model is determined, the effective strain at damage initiation

(ε_i^0) can be determined from Eq. (16). Then the nominal stress-strain relation expressed in Eq. (13) may be determined, and the strain energy release rate in Eq. (14) may also be determined.

For the DCB and SLB specimens, the simulation may be divided into two steps. In the first step, the initiation of interlaminar delamination and the fracture behavior of the 45-egree ply are simulated. The Tsai-Hill failure criterion is used to determine the fracture of the 45-degree ply (kinking into facesheet). After the failure of 45-degree ply according to Tsai-Hill criterion, four-node shell elements used to calculate the stress field near the pre-crack front should be removed. In the second step, the propagation of interlaminar delamination is simulated.

For the EC test specimens, the prediction may be divided into three steps. In the first step, the local buckling of facesheets is predicted. In the second step, the initiation of interlaminar delamination and the fracture behavior of the 45-egree ply are predicted. The Tsai-Hill failure criterion is used to determine the fracture of the 45-degree ply (kinking into facesheet). After the failure of 45-degree ply according to Tsai-Hill criterion, four-node shell elements used to calculate the stress field near the pre-crack front should be removed. In the third step, the propagation of interlaminar delamination is predicted.

5 EC Test of Honeycomb Sandwich Specimen containing Interfacial Debonding

The original dimensions of honeycomb sandwich specimen with a through-width facesheet/core interfacial debonding are 120 x 50 mm. The through-width interfacial debonding is defined by implanting a 0.02 mm thick Teflon sheet between the tool facesheet and honeycomb core before processing. The length of the interfacial debonding is 30mm. The honeycomb sandwich specimen is end-loaded, which requires that the fixture and ends of the honeycomb sandwich are properly aligned and parallel. So width-adjustable U-shaped steel clamps attached to the upper and lower parts of the fixture aid in centering the specimen and prevent end brooming and rotations of the specimen ends. On the one hand, in order to strengthen the mechanical properties of the ends, the honeycomb core of the specimen is removed from the ends of the specimen and replaced by epoxy. On the other hand, in order to keep the upper and lower section of the specimen impregnated with epoxy, the ends of specimen are cut 10 mm on milling machine. So the valid dimensions, namely the unsupported length, of worked specimen are 90 x 50mm. The specimen is compressed axially on Instron 5569 universal machine at a constant displacement of 0.5mm/sec according to the ASTM standard C369-99[18], until failure occurs.

6 Results and Analysis

6.1 Test Result of DCB and SLB specimens

During the process of the DCB and SLB tests, the fracture behavior of pre-crack is recorded real-time by the microscopic Olympus SZX12. The final failure behaviors are shown in Fig. 3. The failure modes, namely IKPs, are observed. The typical characteristics are as follows:

i) The crack propagation does not stay on the facesheet/core interface from the beginning to the end;

(a)

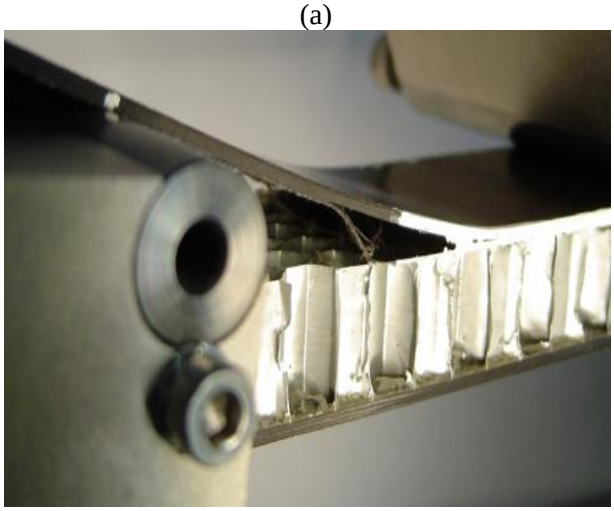

(b)

Fig. 3 Fracture behaviors: (a) DCB specimen and (b) SLB specimen

ii) Prior to crack propagation, interlaminar

delamination occurs between the 45-degree ply and the 0-degree ply;

iii) Along with the initiation of interlaminar delamination, the 45-degree ply begin to fracture at the pre-crack front; in other word, the pre-crack diverges from the facesheet/core interface and kinks into the facesheet;

iv) At the moment that the 45-degree ply fractures completely, there is the unstable propagation of interlaminar delamination at first. Subsequently, the stable propagation of interlaminar delamination occurs.

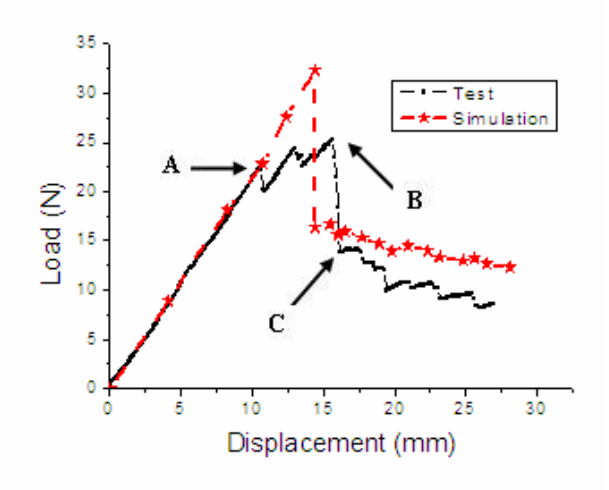

(a)

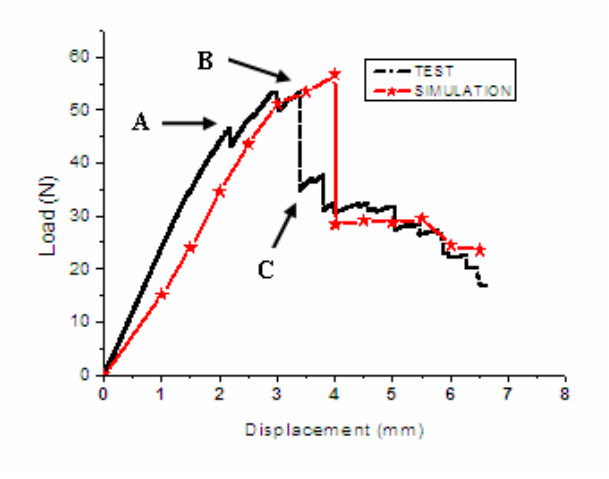

(b)

Fig. 4 Displacement-load curves for DCB and SLB specimens

The load-displacement curve of DCB and SLB experiments are shown in Fig. 4. The process of failure can be approximately categorized into four stages, named as Ⅰ, Ⅱ, Ⅲ and Ⅳ based on the characteristic load-displacement behavior of each stage. In stage Ⅰ, the load increases approximately linearly to point A with the increasing of the cross-head displacement. From point A to point B (namely stage II), the load increases slowly. In this stage, the interlaminar delamination initiation between 45-degree ply and 0-degree ply occurs at the pre-crack front, and the 45-degree ply also begins to fracture along the width direction of the pre-crack front. When the 45-degree ply fractures completely, the load drops rapidly from point B to point C (namely stage III). In stage III, the interlaminar delamination propagates unstably. Beyond the point C, with the interlaminar delamination propagation going on, the load-displacement curve becomes zigzag. In stage IV, the propagation is stable, and the load increases slowly.

6.2 Simulation Result and Analysis of DCB and SLB specimens

In order to simulate the failure modes observed in the DCB and SLB tests, a computational model based on Tsai-Hill failure criterion and cohesive zone model are proposed. In the present simulation, three typical failure modes observed in the tests, such as initiation of interlaminar delamination, fracture of 45-degree ply (kinking into facesheet) and propagation of interlaminar delamination, are successfully simulated.

The load-displacement curve of the DCB and SLB simulations are also shown in Fig.4. For the DCB specimen, before the initiation of interlaminar delamiantion, the difference between simulation and experiment is very small and may be negligible. But with the initiation of interlaminar delamination, the fracture of the 45-degree ply (kinking into facesheet) and the propagation of interlaminar delamination, the load in simulation is higher than the one in the experiment. For the SLB specimen, the difference between simulation and experiment is very obvious. Before the initiation of interlaminar delamiantion, the simulation load is lower than the test load; after the initiation of interlaminar delamiantion, the simulation load is higher than the test load. This might be caused by the assumption in simulation, i.e. the analysis of fracture behavior of the 45-degree ply, as well as uncertainties in experiment. In the simulation, the facture behavior along the width of the pre-crack front is completed synchronously. But in the experiment, the fracture behavior is not synchronous but gradual along the pre-crack front.

6.3 Simulation Result and Analysis of EC specimen

The computational model proposed earlier is used to predict the failure modes of the honeycomb

sandwich containing interfacial debonding under EC loading. According to the simulation result, the failure process of EC specimen may be approximately categorized into four stages, such as the local buckling of facesheet, the initiation of interlaminar delamination, the fracture of 45-degree ply and the propagation of interlaminar delamintion.

The load-displacement curve of EC simulation is shown in Fig. 5. With the increase of compressive displacement, the compressive load is linear increase till the facesheets buckle. When the compressive load reaches 34390N, the local buckling of facesheet occurs within the interfacial debonding region. Subsequently, the interlaminar delamination initiation between 45-degree ply and 0-degree ply occurs near the pre-crack front, and the 45-degree ply also begins to fracture along the width direction of the pre-crack front. In this region, the compressive load beings to increase slowly to the peak value. After the compressive load reaches 41120N, the 45-degree ply fractures completely, the compressive load drops rapidly, the interlaminar delamination propagates unstably. Along with the interlaminar delamination propagation going on, the compressive decrease slowly, the local buckling becomes into the global buckling.

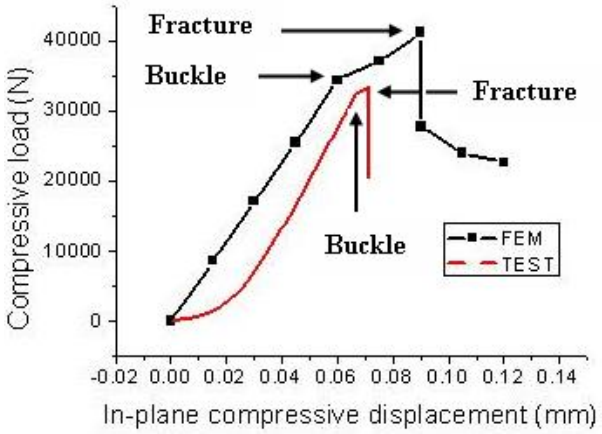

Fig. 5 Load-displacement curves for EC specimen

6.4 Test Result and Analysis of EC specimen

The load-displacement curve of EC test is also shown in Fig. 5. It is evident that the compressive load of test is lower than the one of simulation. The difference of local buckling loads is small, but the difference of fracture of 45-degree ply is very obvious. The reason is on that the failure modes of the test are more complicated than those of the simulation.

Fig. 6 shows the final failure mode of the honeycomb sandwich specimen. Observation of the specimen during EC test has shown that once local buckling of the facesheet occurs within the interfacial debonding region; both fronts of the debonding rapidly propagates towards the ends of the specimen, at the same time. Together with the propagation of interlaminar delamination, the facesheets failed by global Euler buckling which is lateral symmetry. Observation of region A of Fig. 6(a), it is obvious that the interfacial debonding propagated within the facesheet/core interface. However, observation of region B of Fig. 6(a), it is obvious that the interfacial debonding doesn't propagate within the interface, but kinks into the facesheet, and becomes interlaminar delamination. The interlaminar delamination continues to propagate until arrested by the lower clamp. In region C, the interlaminar delamination is also found. In order to study the failure modes, the lower part of tested specimen is magnified in Fig. 6 (b). The failure mode is very evident. The 45-degree ply fractures at the left front of the interfacial debonding, and core also fractures subjected to shear load first and tear load subsequently.

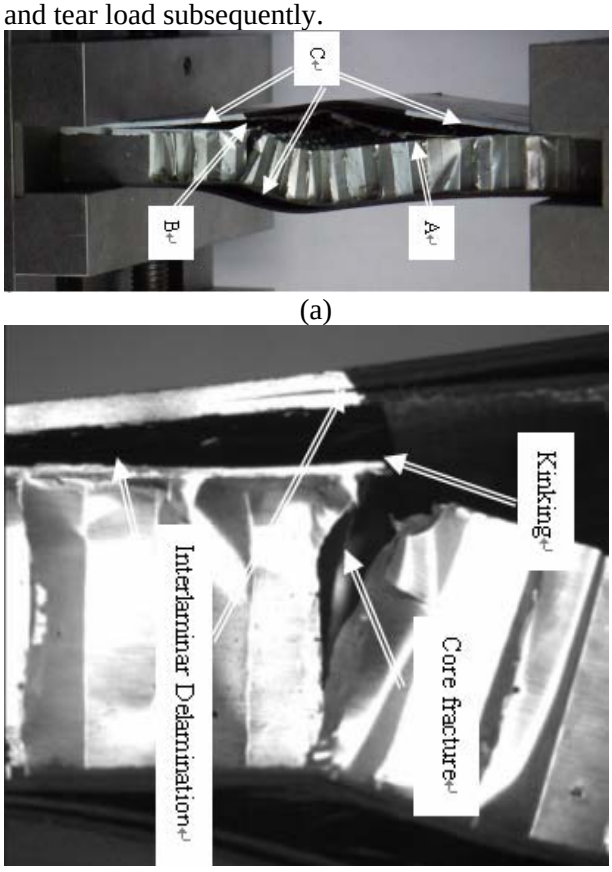

(a)

(b)

Fig. 6 Final failure mode of honeycomb sandwich under the EC test for (a) Global and (b) Local

7 Conclusions

The failure behavior of honeycomb sandwich with facesheet/core interfacial debonding is investigated experimentally and numerically. The following conclusions are obtained:

a) In the DCB and SLB tests, the interfacial debonding doesn't propagate within the facesheet/core interface, but kinks into facesheet, and develops into the interlaminar delamination;

b) In the DCB and SLB simulations, the failure modes found in the tests are successfully simulated, so the computional model based on the Tsai-Hill failure criterion and the cohesive zone model is reasonable;

c) According to the EC simulation result, the failure process may be approximately categorized into four stages, such as the local buckling of facesheet, the initiation of interlaminar delamination, the fracture of 45-degree ply and the propagation of interlaminar delamintion;

d) Although the failure modes occurred in the EC test are very complicated, the main failure modes predicted in the EC simulation are all observed during the process of the EC test;

e) So, the computational model based on the Tsai-Hill failure criterion and the cohesive zone model is reasonable to predict the failure modes of honeycomb sandwich with interfacial debonding or interlaminar delamination.

References

[1] Abrate S. Localized impact on sandwich structures with laminated facings. Appl Mech Rev, Vol. 50, pp69-82, 1997.

[2] Prasad S. and Carlsson L. A. Debonding and crack kinking in foam core sandwich beams-I. Analysis of fracture specimens. Eng Fract Mech, Vol. 47, No. 6, pp813-24, 1994.

[3] Prasad S. and Carlsson L. A. Debonding and crack kinking in foam core sandwich beams-II. Experimental investigation. Eng Fract Mech, Vol. 47, No. 6, pp825-41, 1994.

[4] Li X. and Carlsson L. A. The tilted sandwich debond (TSD) specimen for face/core interface fracture characterization. J Sandwich Struct Mater, Vol. 1, No. 1, pp60-75, 1999.

[5] Cantwell W. J. and Davies P. A. A test technique for assessing core-skin adhesion in composite sandwich structures. J Mater Sci Lett, Vol. 13, No. 3, pp203-5, 1994.

[6] Cantwell W. J. and Davies P. A. A study of skin-core adhesion in glass reinforced sandwich materials. Appl Compos Mater, Vol. 3, No. 6, pp407-20, 1996.

[7] Cantwell W. J., Scudamore R., Ratcliffe J. and Davibes P. Interfacial fracture in sandwich laminates. Compos Sci Technol, Vol. 59, No. 14, pp2079-85, 1999.

[8] Ural A., Zehnder A. T., and Ingraffea A. R. Fracture mechanics approach to facesheet delamination in honeycomb: Measurement of Energy Release Rate of the Adhesive Bond. Eng Fract Mech, Vol. 70, pp93-103, 2003.

[9] Paik J. K., Thayamballi A. K. and Kim G. S. The strength characteristics of aluminum honeycomb sandwich panels. Thin-walled Structures, Vol. 35, pp205-31, 1999.

[10] Gdoutos E. E., Daniel I. M. and Wang K. A. Compression facing wrinkling of composite sandwich structures. Mechanics of Materials, Vol. 35, pp511-22, 2003.

[11] Kwon Y. W., Yoon S. H. and Sistare P. J. Compressive failure of carbon-foam sandwich composites with holes and/or partial delamiantion. Composites Structures, Vol. 38, pp573-80, 1997.

[12] Vadakke V. and Carlsson L. A. Experimental investigation of compression failure of sandwich specimens with face/core debond. Composites: Part B, Vol. 35, pp583-90, 2004.

[13] Dugdale D. S. Yielding of Sheets Containing Slits. Journal of Mechanics and Physics of Solids, Vol. 8, pp100-4, 1960.

[14] Barenblatt G. I. The mathematical theory of equilibrium cracks in brittle fracture. Advances in Applied Mechanics, Vol. 2, pp55-129.

[15] Sayed E. and Sridharan S. Cohesive layer models for predicting delamination growth and crack kinking in sandwich structures. Int J Fract, Vol. 117, pp63-84, 2002.

[16] Han T. S., *et. al*. Delamination buckling and propagation analysis of honeycomb panels using a cohesive element approach. Int J Fract, Vol. 115, pp101-23, 2002.

[17] C297-94, Standard test method for flatwise tensile strength of sandwich constructions. Philadelphia: American Society for Testing and Materials, 1994.

[18] C364-99, Standard test method for edgewise compressive strength of sandwich constructions. Philadelphia: American Society for Testing and Materials, 1999.